Growth direction and morphology of ZnO nanobelts revealed by combining *in situ* atomic force microscopy and polarized Raman spectroscopy

Marcel Lucas,[1,*] Zhong Lin Wang,[2] and Elisa Riedo[1,†]
[1]*School of Physics, Georgia Institute of Technology, Atlanta, Georgia 30332-0430, USA*
[2]*School of Materials Science and Engineering, Georgia Institute of Technology, Atlanta, Georgia 30332-0245, USA*
(Received 26 June 2009; revised manuscript received 28 September 2009; published 14 January 2010)

Control over the morphology and structure of nanostructures is essential for their technological applications, since their physical properties depend significantly on their dimensions, crystallographic structure, and growth direction. A combination of polarized Raman (PR) spectroscopy and atomic force microscopy (AFM) is used to characterize the growth direction, the presence of point defects and the morphology of individual ZnO nanobelts. PR-AFM data reveal two growth modes during the synthesis of ZnO nanobelts by physical vapor deposition. In the thermodynamics-controlled growth mode, nanobelts grow along a direction close to [0001], their morphology is growth-direction dependent, and they exhibit no point defects. In the kinetics-controlled growth mode, nanobelts grow along directions almost perpendicular to [0001], and they exhibit point defects.

DOI: 10.1103/PhysRevB.81.045415 PACS number(s): 61.46.−w, 61.72.Dd, 78.30.Ly, 81.10.−h

I. INTRODUCTION

Control over the morphology and structure of nanostructured materials is essential for the development of future devices, since their physical properties depend on their dimensions and crystallographic structure.[1–15] In particular, the growth direction of single-crystal nanostructures affects their piezoelectric,[1,2] transport,[3] catalytic,[4] mechanical,[5–9] optoelectronic,[10] and tribological properties.[11] ZnO nanostructures with various morphologies (wires, belts, helices, rings, tubes,…) have been successfully synthesized in solution and in the vapor phase,[14–19] but little is known about their growth mechanism, particularly in a process not involving catalyst particles.[17] Understanding the growth mechanism and determining the decisive parameters directing the growth of nanostructures and tailoring their morphology is essential for the use of ZnO nanobelts as power generators or electromechanical systems.[1,2,5,6] From a theoretical standpoint, a shape-dependent thermodynamic model showed that the morphology of ZnO nanobelts grown in equilibrium conditions depends on their growth direction, but the role of defects was not considered.[20] Experimentally, it was shown that the growth direction of ZnO nanostructures can be directed by the synthesis conditions, such as the oxygen content in the furnace.[19] A previous study combining scanning electron microscopy and x-ray diffraction suggested a growth-direction-dependent morphology.[20] An atomic force microscopy (AFM) combined with transmission electron microscopy also suggested that the morphology of ZnO nanobelts is correlated with their growth direction and highlighted the potentially important role of planar defects.[5]

Growth modes out of thermodynamic equilibrium and the role of point defects[5,17] are particularly challenging to investigate experimentally,[21] due to the lack of appropriate experimental techniques. Electron microscopy can determine the crystallographic structure and morphology of conductive nanomaterials,[3,17,22–24] but is not suitable for the characterization of point defects, especially when their distribution is disordered.[17,22–24] Raman spectroscopy has been used for the characterization of the structure of carbon nanotubes,[25,26] the identification of impurities,[27] and the determination of the crystal structure[28] and growth direction of individual single-crystal nanowires.[29] Recently, polarized Raman (PR) spectroscopy has been coupled to AFM to study *in situ* the interplay between point defects and mechanical properties of ZnO nanobelts.[30]

Here, PR-AFM is used to study the growth mechanism and the relationship between growth direction, point defects, and morphology of individual ZnO nanobelts. The morphology of an individual ZnO nanobelt is determined by AFM, while the growth direction and randomly distributed defects in the same individual nanobelt are characterized by polarized Raman spectroscopy.

II. EXPERIMENTAL

The ZnO nanobelts were prepared by physical vapor deposition (PVD) without catalysts following the method described in Ref. 17. The ZnO nanobelts were deposited on a glass cover slip, which was glued to a Petri dish. The rotatable Petri dish was then placed on a sample plate under an Agilent PicoPlus AFM equipped with a scanner of 100 $\times 100$ μm^2 range. Topography images of the ZnO nanobelts were collected in the contact mode with CONTR probes (NanoWorld AG, Neuchâtel, Switzerland) of normal spring constant 0.21 N/m at a set point of 2 nN. The AFM was placed on top of an Olympus IX71 inverted optical microscope that is coupled to a Horiba Jobin-Yvon LabRam HR800. PR spectra were recorded in the backscattering geometry using a 40× (0.6 NA) objective focusing a laser beam of wavelength 785 nm on the sample to a power density of about 10^5 W/cm^2 and a spot size of about 2 μm. The incident polarization direction can be rotated continuously with a half-wave plate. The scattered light was analyzed along one of two perpendicular directions by a polarizer at the entrance of the spectrometer. The intensity, center, and width of the Raman bands were obtained by fitting the spectra with Lorentzian lines. The polarization dependence of the quantum efficiency of the Raman spectrometer was tested by measuring the intensity variations of the 377, 409,

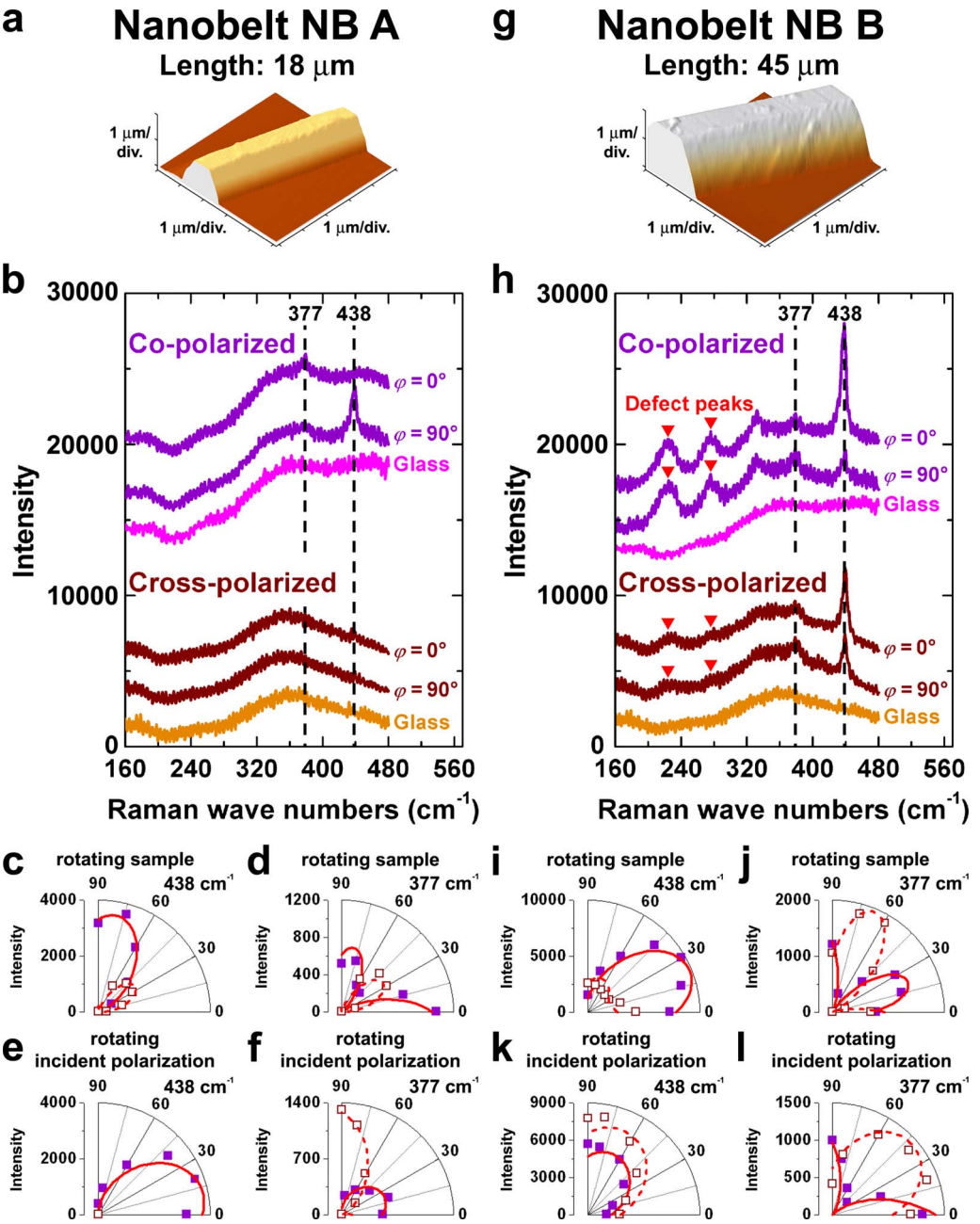

FIG. 1. (Color online) PR-AFM results on individual ZnO nanobelts. (a) AFM topography image, (b) typical PR spectra for different sample orientations φ and polarization configurations, and (c)–(f) polar plots of the angular dependence of the Raman intensities for the nanobelt NB A. (g) AFM topography image, (h) typical PR spectra, and (i)–(l) polar plots of the angular dependence of the Raman intensities for the nanobelt NB B. The Raman spectra in (h) exhibit peaks centered at 224 and 275 cm^{-1} (triangles) that are characteristic of defects in the nanobelt NB B. The Raman spectra are offset vertically for clarity. In (c), (d), (i), and (j), the nanobelt axis is rotated in a fixed polarization configuration (solid squares: copolarized; open squares: cross polarized) and is parallel to the incident polarization for φ=0°. In (e), (f), (k), and (l), the incident polarization is rotated, while the analyzed polarization and the nanobelt axis are fixed. In (e), (f), (k), and (l), at the angle 0°, the nanobelt is perpendicular to the incident polarization and the incident and analyzed polarizations are parallel (solid squares) or perpendicular (open squares). Typical Raman spectra of the glass cover slip in the copolarized and cross-polarized configurations are shown as a reference in (b) and (h), respectively.

and 438 cm^{-1} bands from two bulk ZnO crystals (*c*-plane and *m*-plane ZnO crystals, MTI Corporation). The PR data from bulk crystals were successfully fitted using group theory and crystal symmetry[28] without further calibration of the spectrometer or data correction.

III. RESULTS AND DISCUSSION

AFM images and PR data of two individual ZnO nanobelts are presented in Fig. 1. These nanobelts have different cross-sections, 1320×1080 nm^2 (nanobelt labeled NB A)

[Figs. 1(a)–1(f)] and 2270×1760 nm^2 (labeled NB B) [Figs. 1(g)–1(l)], but similar width-to-thickness ratio, w/t, around 1.2. The glass cover slip gives rise to a weak polarization-dependent Raman band centered around 350 cm^{-1} [Figs. 1(b) and 1(h)]. In ambient conditions, ZnO has a wurtzite structure (space group C_{6v}^4). The 377 and 438 cm^{-1} bands correspond to the Raman-active A_1 and E_2 modes, respectively.[14,27,28] A comparison of the PR spectra for NB A and NB B reveals additional Raman bands around 224 and 275 cm^{-1} for the larger NB B. These bands were assigned to the presence of randomly distributed point defects, such as oxygen vacancies or impurities, in doped or ion-implanted ZnO crystals.[14,27,31]

Four series of Raman spectra were collected on all ZnO nanobelts with an exposure time of 20 min each, in different polarization configurations. In the first two series, the nanobelt axis was rotated in a fixed polarization configuration, either copolarized or cross-polarized [Figs. 1(c), 1(d), 1(i), and 1(j)]. The ZnO nanobelt was rotated from 0° (where the nanobelt axis was parallel to the incident polarization) to 90°. After each rotation of the sample, the laser spot was recentered on the same nanobelt and at the same location along the nanobelt. In the next two series, the incident polarization was rotated, while the analyzed polarization and the nanobelt axis were fixed [Figs. 1(e), 1(f), 1(k), and 1(l)]. The incident polarization was rotated from 0°, where the nanobelt was perpendicular to the incident polarization, to 90°. The center and width of the peaks at 377 and 438 cm^{-1} remained constant for all orientations and polarization configurations. The error on the intensity values is ± 100 counts. To determine the angle θ between the nanobelt long axis (or growth direction) and the c axis of the constituting ZnO wurtzite structure,[28,29] the angle between the ZnO nanobelt axis and the projection of the c axis of its ZnO wurtzite structure on the substrate is first determined by fitting the PR intensity variations of the 438 cm^{-1} peak to the predictions from group theory and crystal symmetry.[28] The angle between the c axis of the ZnO wurtzite structure and the normal to the substrate is then determined graphically by plotting the expected angular dependence of the 377 and 438 cm^{-1} peaks for all four series of PR data with different magnitudes and phases of the Raman tensor components.[29] The ZnO nanobelts studied here have dimensions over 300 nm, so no enhancement of the Raman signal is expected from their aspect ratio.[32] From the PR data, it was found that NB A grew along the c direction (θ=6°), while the growth direction of NB B makes an angle θ=71° with the c direction. The error, mainly from the determination of the out-of-plane inclination, is estimated to be 15°.

The angle θ and the presence of defects are characterized for a total of 21 ZnO nanobelts of different dimensions and the results are reported in Figs. 2 and 3. The 377 cm^{-1} peak was not observed in most nanobelts with strong defect peaks, in which case the growth direction was solely determined from the angular dependencies of the 438 cm^{-1} peak. We find that the growth direction and the presence of randomly distributed defects are correlated with the nanobelt length (Fig. 2). Nanobelts longer than 40 μm exhibit defect peaks and grow with $\theta > 75° \pm 15°$, along a direction almost perpendicular to the c direction, while the shorter nanobelts

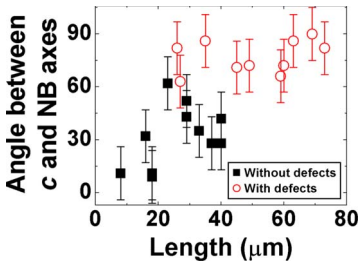

FIG. 2. (Color online) Angle between the ZnO nanobelt axis (growth direction) and the c axis of the constituting ZnO wurtzite structure, as a function of the nanobelt length. The nanobelts exhibiting defect peaks in their Raman spectra are indicated by open circles, and the nanobelts without defect peaks by solid squares.

have no defects and grow mostly along the c direction. This correlation with the length translates into a similar correlation with the volume.

To further investigate the relation between structure and morphology, θ is plotted as a function of w/t in Fig. 3. The results indicate that the nanobelts without defects have a morphology that is related to the growth direction, with their w/t increasing with θ. In contrast, nanobelts with defects grow with $\theta > 60°$ independently of w/t. These results are consistent with the observation of a stacking fault over the entire length of nanobelts grown along the $[01\bar{1}0]$ direction.[5,17]

The ZnO nanobelts were synthesized by a PVD process without catalysts, and no particle was observed at the ends of nanobelts. Therefore, their growth mechanism differs from the vapor-liquid-solid process, which was proposed for syntheses assisted by catalysts. The results presented in Figs. 2 and 3 suggest the coexistence of two growth modes for PVD-grown ZnO nanobelts: one slow-growth mode in quasiequilibrium conditions (short nanobelts) and another fast-growth mode in nonequilibrium conditions (long nanobelts). ZnO nanostructures grow preferentially along the c direction.[14,17] However, other growth directions, perpendicular to the $(\bar{1}2\bar{1}0)$, $(11\bar{2}0)$, and $(01\bar{1}2)$ planes, have been observed.[17–20] In quasiequilibrium slow-growth conditions, thermodynamics would favor growth directions, such as the c direction, that are normal to high-energy surfaces, such as the $\pm(0001)$ polar planes,[20] to minimize their area and the

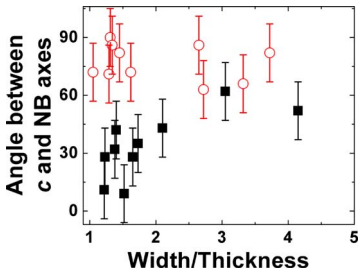

FIG. 3. (Color online) Angle between the ZnO nanobelt axis and the c axis of the constituting ZnO wurtzite structure, as a function of the nanobelt width-to-thickness ratio. The nanobelts exhibiting defect peaks in their Raman spectra are indicated by open circles, and the nanobelts without defect peaks by solid squares.

total free energy. Other polar surfaces or surfaces with a high density of Zn or O atoms are the $\{10\bar{1}2\}$ and $\{10\bar{1}1\}$ planes. The directions normal to these planes form with the c direction angles of 0°, 43°, and 62°, which are consistent with the observed θ values for short (slow-growth) nanobelts with no point defects (solid squares in Fig. 2). However, thermodynamics alone cannot explain growth directions perpendicular to low-energy surfaces, such as the $(\bar{1}2\bar{1}0)$ and $(11\bar{2}0)$ planes in ZnO nanobelts, or the synthesis of In_2O_3 and CdO nanobelts that are enclosed by crystallographically equivalent faces.[33]

A vapor-solid process was introduced to explain the growth of ZnO nanobelts without catalyst particles, where kinetics also plays a role in the nanostructure growth.[33,34] In the vapor-solid growth mechanism, the two-dimensional nucleation probability on the surface of a whisker is a function of the surface energy of the solid whisker, the temperature and the supersaturation ratio (ratio between the actual pressure and the equilibrium pressure) of the vapor phase.[34] It was concluded that a high temperature and large supersaturation ratio (nonequilibrium conditions) leads to the formation of sheetlike structures (high w/t), while a low temperature and small supersaturation ratio (quasiequilibrium conditions) leads to the preferential growth of wirelike structures (low w/t).[33] Experimental studies using similar equipment have shown that, inside the furnace, the temperature and the ZnO vapor pressure decreases as the distance to the source (alumina boat containing ZnO powder) increases.[35–37] Various morphologies of ZnO nanostructures, with a wide range of aspect ratios, were formed depending on the substrate temperature and distance to the source.[35–37] ZnO nanobelts with high w/t were most likely observed on the substrate located close to the ZnO source at a higher temperature, and that observation was made whether a gold catalyst was added to the substrate or not.[37]

Growth at high temperatures and large supersaturation ratio (nonequilibrium conditions) also leads to ZnO nanostructures with a high density of defects, due to the higher deposition rate of molecular ZnO from the vapor.[38] The introduction of defects, particularly at high temperatures, can increase the growth rate of ZnO nanostructures and the overall size of the synthesis products.[39,40] More importantly, the introduction of points defects, such as oxygen vacancies or zinc interstitials,[18,41] significantly affects the surface energy of the nanostructure faces, thus modifying the growth habit of the nanostructure.[19] The growth habit along the c direction is due to the preferential adsorption of molecular ZnO on the Zn-terminated polar (0001) surface.[15] The presence of defects reduces the polarity of the (0001) surface and thus the deposition rate of molecular ZnO.[19] A modification of the growth habit is due to the change in relative growth rates of the different crystallographic faces.[42] Once the growth along the c direction is inhibited by defects,[19] or a capping agent,[43,44] the growth kinetics along directions other than the c direction is then enhanced, in particular directions perpendicular to the c direction, leading to the synthesis of ZnO nanostructures with high w/t.[5,6,43,44] These results confirm the enhanced reactivity of polar surfaces and highlight the connection between defects, polar surfaces, and growth conditions.

IV. SUMMARY

In summary, a combination of polarized Raman spectroscopy and AFM reveals two growth modes during the PVD synthesis of ZnO nanobelts, one controlled by thermodynamics and another one by kinetics. In the thermodynamically controlled growth mode, nanobelts grow mostly along the c direction with no point defects and exhibit a growth-direction-dependent morphology. In the kinetically controlled growth mode, nanobelts grow along directions forming angles larger than 60° with the c direction and exhibit point defects. These findings are important to properly control the growth direction of ZnO nanobelts for their applications in devices.

ACKNOWLEDGMENT

The authors acknowledge the financial support from the Department of Energy under Grant No. DE-FG02-06ER46293.

*marcel.lucas@gatech.edu
†elisa.riedo@physics.gatech.edu

[1] Y. Qin, X. Wang, and Z. L. Wang, Nature (London) **451**, 809 (2008).
[2] X. Wang, J. Song, J. Liu, and Z. L. Wang, Science **316**, 102 (2007).
[3] H. Peng, C. Xie, D. T. Schoen, and Y. Cui, Nano Lett. **8**, 1511 (2008).
[4] U. Diebold, Surf. Sci. Rep. **48**, 53 (2003).
[5] M. Lucas, W. J. Mai, R. Yang, Z. L. Wang, and E. Riedo, Nano Lett. **7**, 1314 (2007).
[6] M. Lucas, W. J. Mai, R. Yang, Z. L. Wang, and E. Riedo, Philos. Mag. **87**, 2135 (2007).
[7] M. D. Uchic, D. M. Dimiduk, J. N. Florando, and W. D. Nix, Science **305**, 986 (2004).
[8] M. Lucas, A. M. Leach, M. T. McDowell, S. E. Hunyadi, K. Gall, C. J. Murphy, and E. Riedo, Phys. Rev. B **77**, 245420 (2008).
[9] M. Lucas, K. Gall, and E. Riedo, J. Appl. Phys. **104**, 113515 (2008).
[10] D.-S. Yang, C. Lao, and A. H. Zewail, Science **321**, 1660 (2008).
[11] M. Dienwiebel, G. S. Verhoeven, N. Pradeep, J. W. M. Frenken, J. A. Heimberg, and H. W. Zandbergen, Phys. Rev. Lett. **92**, 126101 (2004).
[12] C. Q. Chen, Y. Shi, Y. S. Zhang, J. Zhu, and Y. J. Yan, Phys. Rev. Lett. **96**, 075505 (2006).
[13] B. Wen, J. E. Sader, and J. J. Boland, Phys. Rev. Lett. **101**, 175502 (2008).
[14] Ü. Özgür, Ya. I. Alivov, C. Liu, A. Teke, M. A. Reshchikov,

S. Doğan, V. Avrutin, S.-J. Cho, and H. Morkoç, J. Appl. Phys. **98**, 041301 (2005).
[15] Z. L. Wang, J. Phys.: Condens. Matter **16**, R829 (2004).
[16] G. R. Li, T. Hu, G. L. Pan, T. Y. Yan, X. P. Gao, and H. Y. Zhu, J. Phys. Chem. C **112**, 11859 (2008).
[17] Z. W. Pan, Z. R. Dai, and Z. L. Wang, Science **291**, 1947 (2001).
[18] Q. Yang, K. Tang, J. Zuo, and Y. Qian, Appl. Phys. A: Mater. Sci. Process. **79**, 1847 (2004).
[19] X. N. Zhang, C. R. Li, and Z. Zhang, Appl. Phys. A: Mater. Sci. Process. **82**, 33 (2006).
[20] A. S. Barnard, Y. Xiao, and Z. Cai, Chem. Phys. Lett. **419**, 313 (2006).
[21] X. Dou, G. Li, and H. Lei, Nano Lett. **8**, 1286 (2008).
[22] P. Poncharal, Z. L. Wang, D. Ugarte, and W. A. De Heer, Science **283**, 1513 (1999).
[23] A. M. Minor, J. W. Morris, and E. A. Stach, Appl. Phys. Lett. **79**, 1625 (2001).
[24] B. Varghese, Y. Zhang, L. Dai, V. B. C. Tan, C. T. Lim, and C.-H. Sow, Nano Lett. **8**, 3226 (2008).
[25] M. Lucas and R. J. Young, Phys. Rev. B **69**, 085405 (2004).
[26] M. Lucas and R. J. Young, Compos. Sci. Technol. **67**, 2135 (2007).
[27] H. Zhong, J. Wang, X. Chen, Z. Li, W. Xu, and W. Lu, J. Appl. Phys. **99**, 103905 (2006).
[28] C. A. Arguello, D. L. Rousseau, and S. P. S. Porto, Phys. Rev. **181**, 1351 (1969).
[29] T. Livneh, J. Zhang, G. Cheng, and M. Moskovits, Phys. Rev. B **74**, 035320 (2006).
[30] M. Lucas, Z. L. Wang, and E. Riedo, Appl. Phys. Lett. **95**, 051904 (2009).
[31] F. J. Manjón, B. Marí, J. Serrano, and A. H. Romero, J. Appl. Phys. **97**, 053516 (2005).
[32] H. M. Fan, X. F. Fan, Z. H. Ni, Z. X. Shen, Y. P. Feng, and B. S. Zou, J. Phys. Chem. C **112**, 1865 (2008).
[33] Z. R. Dai, Z. W. Pan, and Z. L. Wang, Adv. Funct. Mater. **13**, 9 (2003).
[34] J. M. Blakely and K. A. Jackson, J. Chem. Phys. **37**, 428 (1962).
[35] C. Li, G. Fang, Q. Fu, F. Su, G. Li, X. Wu, and X. Zhao, J. Cryst. Growth **292**, 19 (2006).
[36] Y. Yan, L. Zhou, L. Yu, and Y. Zhang, Appl. Phys. A: Mater. Sci. Process. **93**, 457 (2008).
[37] S. L. Mensah, V. K. Kayastha, and Y. K. Yap, J. Phys. Chem. C **111**, 16092 (2007).
[38] T.-W. Kim, T. Kawazoe, S. Yamazaki, M. Ohtsu, and T. Sekiguchi, Appl. Phys. Lett. **84**, 3358 (2004).
[39] G. Dhanaraj, M. Dudley, D. Bliss, M. Callahan, and M. Harris, J. Cryst. Growth **297**, 74 (2006).
[40] Y. Huang, J. He, Y. Zhang, Y. Dai, Y. Gu, S. Wang, and C. Zhou, J. Mater. Sci. **41**, 3057 (2006).
[41] J. N. Zeng, J. K. Low, Z. M. Ren, T. Liew, and Y. F. Lu, Appl. Surf. Sci. **197-198**, 362 (2002).
[42] W.-J. Li, E.-W. Shi, W.-Z. Zhong, and Z.-W. Yin, J. Cryst. Growth **203**, 186 (1999).
[43] L. Xu, Y. Guo, Q. Liao, J. Zhang, and D. Xu, J. Phys. Chem. B **109**, 13519 (2005).
[44] Y. Peng, A.-W. Xu, B. Deng, M. Antonietti, and H. Cölfen, J. Phys. Chem. B **110**, 2988 (2006).